### 九州大学学術情報リポジトリ Kyushu University Institutional Repository

# Aging Effect on Microstructure of Cold Groove-Rolled $\alpha'$ -Type Ti-12 mass%V-2 mass%Al Alloys Studied by Transmission Electron Microscopy

Sato, Kazuhisa Institute for Materials Research, Tohoku University

Matsumoto, Hiroaki Institute for Materials Research, Tohoku University

Chiba, Akihiko Institute for Materials Research, Tohoku University

Konno, Toyohiko J. Institute for Materials Research, Tohoku University

https://hdl.handle.net/2324/7393052

出版情報: MATERIALS TRANSACTIONS. 55 (5), pp. 763-767, 2014-05-01. 日本金属学会

バージョン:

権利関係: © 2014 The Japan Institute of Metals and Materials



## Aging Effect on Microstructure of Cold Groove-Rolled $\alpha'$ -Type Ti–12 mass %V–2 mass %Al Alloys Studied by Transmission Electron Microscopy

Kazuhisa Sato\*1, Hiroaki Matsumoto\*2, Akihiko Chiba and Toyohiko J. Konno

Institute for Materials Research, Tohoku University, Sendai 980-8577, Japan

Microstructure and phase decomposition of hexagonal  $\alpha'$  martensite in cold groove rolled (CGR) Ti-12 mass%V-2 mass%Al alloys have been studied by transmission electron microscopy and electron diffraction. Acicular structure of the  $\alpha'$  martensite changes into equiaxed  $\alpha'$  grains by CGR with a cold reduction of 75%. After aging at 573 K for 500 h, local Moiré fringes disappear and diffraction rings become sharp due to recovery. However, Vickers hardness also increased in spite of the recovery. Partitioning of solute atoms and/or formation of fine precipitates can be possible cause for the observed age-hardening. Although a CGR alloy is characterized by a microstructure with polycrystalline equiaxed grains, following orientation relationship is locally observed between  $\beta$  precipitates and  $\alpha$  grains after aging at 673 K:  $(101)_{\beta}$  //  $(01\overline{11})_{\alpha}$ ,  $[010]_{\beta}$  //  $[10\overline{11}]_{\alpha}$ . Electron tomography revealed a heterogeneous nucleation and growth of  $\beta$  precipitates in the deformed  $\alpha'$  matrix. [doi:10.2320/matertrans.M2013463]

(Received December 26, 2013; Accepted February 20, 2014; Published April 25, 2014)

**Keywords:**  $\alpha'$ -martensite, titanium-vanadium-aluminum, cold groove rolling, recovery, transmission electron microscopy (TEM), electron tomography

#### 1. Introduction

Titanium alloys are widely used in various fields, such as aerospace and automobile industries, and biomedical applications, 1-3) due to their high specific strength and corrosion resistance. Among Ti-alloy systems, Ti-V alloys composed of hexagonal  $\alpha'$  martensite possess low Young's moduli ( $\sim$ 60 GPa) and high strength ( $\sim$ 1000 MPa), and exhibit a good machinability for cold groove rolling (CGR).<sup>4–7)</sup> The  $\alpha'$ martensite is formed by solution treatment above the  $\beta$ transus followed by quenching (hereafter, STQ).<sup>1)</sup> Recent studies have revealed that  $\alpha'$ -type Ti–12 mass%V–2 mass%Al (Ti-12V-2Al) alloys show more than 90% of reduction by cold rolling (termed as  $\alpha'$ -processing<sup>6,7)</sup>), while equilibrium alloys composed of the  $\alpha$  (hexagonal close packed: hcp) and  $\beta$  (body centered cubic: bcc) phases show reduction less than 45%.8 A proposed deformation mechanism for the  $\alpha'$ -type Ti-V-Al alloys is as follows: basal  $\langle a \rangle$  slip and  $\{10\overline{1}1\}$ twining are activated in the initial stage of plastic deformation, and then  $\langle a+c \rangle$  slip begins to be activated as strain increases by plastic deformation.<sup>8)</sup> After cold rolling, original microstructures with acicular martensite changes to that with fine grains of dislocation cell elongated along the rolling direction.<sup>6,7)</sup> It is expected that characterization of deformed and subsequently aged microstructures will provide an insight into the deformation mechanism from structural viewpoints. There are several reports on  $\alpha$  precipitates in the  $\beta$  matrix, <sup>9,10)</sup> while the reverse case, i.e.,  $\beta$  precipitates in  $\alpha'$ matrix has not been clarified in detail.

The authors have studied phase separation of  $\alpha'$  martensite in Ti–12V–2Al STQ alloys towards equilibrium  $\alpha$  and  $\beta$  phases on aging. We have revealed that significant agehardening can be attributed to fine  $\beta$  precipitates nucleated

inside primary  $\alpha'$  martensite plates.<sup>11)</sup> The CGR alloys, composed of ultrafine  $\alpha'$  grains, also show an increase of Vickers hardness and Young's modulus by aging at 573 K, while their origin has not been clarified yet.

In this study we focused on aging effects on microstructure of cold worked Ti–12V–2Al alloys composed of ultrafine  $\alpha'$  grains using transmission electron microscopy (TEM) and electron diffraction.

#### 2. Experimental Procedure

Ti-12 mass%V-2 mass%Al alloys were prepared by arc melting in an argon atmosphere using high purity Ti, V, and Al, followed by homogenization at 1423 K for 24 h. 6,7) The homogenized rod shaped alloys with 12 mm in diameter were cold groove-rolled to cylindrical shape with 10 mm in diameter. The cylindrical alloys were then solution treated at 1223 K (above the  $\beta$  transus) for 2 h in an evacuated quartz tube, and quenched into ice water (STQ). The quenched rods were again cold groove rolled to the final diameter of 5 mm (a cold reduction of 75%). The CGR bars were heat treated at 573 K for 0.5–500 h, at 673 K for 24 h, or at 773 K for 24 h. Chemical analysis for the CGR alloy showed carbon, nitrogen and oxygen contents be 0.025 mass% C, 0.011 mass% N and 0.227 mass% O, respectively, after aging at 573 K for 500 h. Thin specimens for electron microscopy were prepared by mechanical polishing followed by electropolishing, and completed by Ar ion milling. The specimen surface was perpendicular to the rolling direction (RD).

Microstructures of these alloys were observed using JEOL JEM-2000FX (200 kV) and JEM-3011 (300 kV) TEMs. High-resolution TEM (HRTEM) and scanning TEM (STEM) images were obtained by using an FEI Titan 80-300 (S)TEM operating at 300 kV with a field emission gun and an aberration corrector for objective lens (CEOS image corrector). Elemental analyses were carried out using an energy dispersive X-ray spectrometer (EDS) attached to the

<sup>\*1</sup>Corresponding author, E-mail: ksato@imr.tohoku.ac.jp

<sup>\*2</sup>Present address: Department of Advanced Materials Science, Kagawa University, Takamatsu 761-0396, Japan

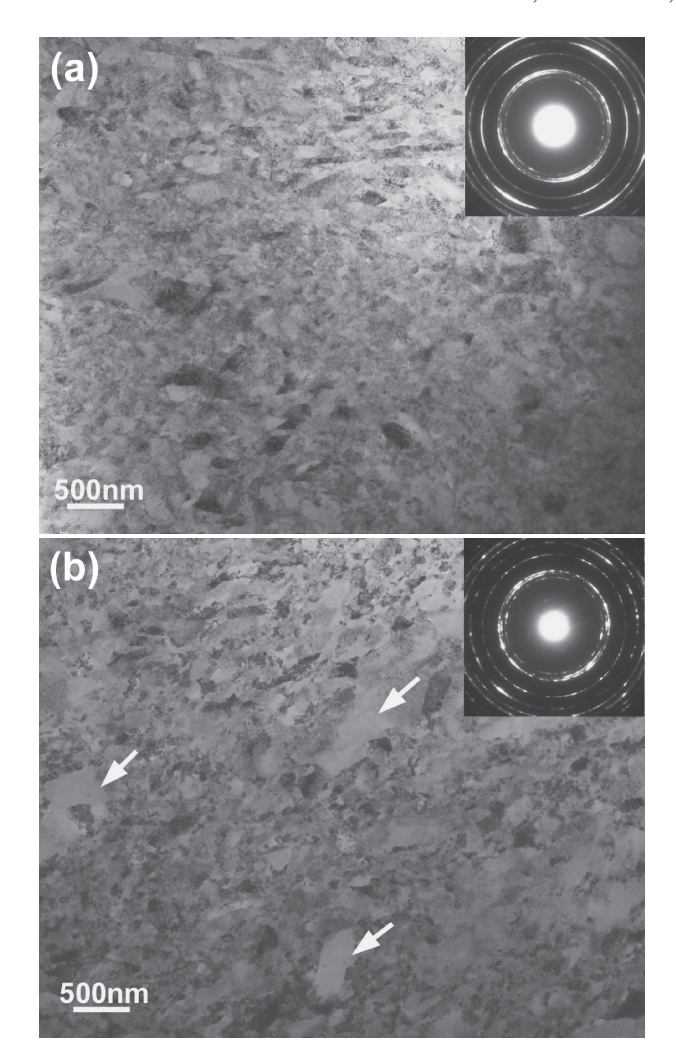


Fig. 1 BF-TEM images and corresponding SAED patterns of cold rolled Ti–12 mass%V–2 mass%Al alloys by CGR with a reduction of 75%, (a) as-rolled, and (b) after aging at 573 K for 500 h. The arrows indicate large grains, while a majority of the alloy is still composed of fine equiaxed grains.

300 kV-(S)TEM. A single-tilt holder (Fischione model 2020) was used for tilt-series acquisition with the maximum tilt angle of 70°. We used an FEI Inspect3D software package for subsequent data processing, including alignment of the tilt axis for the obtained data set based on an iterative cross-correlation technique, and 3D reconstruction based on a weighted back-projection (WBP) method.

#### 3. Results and Discussion

Figure 1(a) shows a bright-field (BF) TEM image and a corresponding selected area electron diffraction (SAED) pattern of the as-rolled alloy taken from an area  $\sim\!3.5\,\mu m$  in diameter. Acicular martensite microstructure of the asquenched alloy<sup>6,7,11)</sup> is totally changed into equiaxed grains, typically 100–300 nm in size, due to severe plastic deformation of martensite plates by CGR with a cold reduction of 75%. As seen, Debye–Scherrer rings indicate formation of polycrytsalline fine grains. Figure 1(b) shows a BF-TEM image and a corresponding SAED pattern of the CGR alloy after aging at 573 K for 500 h. Although a few large grains exist as indicated by arrows, a majority of the alloy is still composed of fine equiaxed grains and extensive grain growth

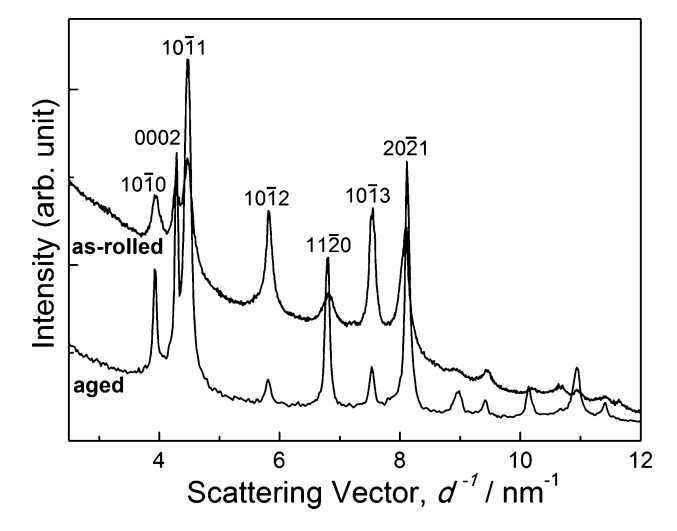


Fig. 2 SAED intensity profiles for as-rolled and aged alloys after aging at  $573\,\mathrm{K}$  for  $500\,\mathrm{h}$  measured in the radial direction.

was not occurred at this stage. Debye–Scherrer rings in the attached SAED pattern became sharp compared to those observed for the as-rolled specimen (Fig. 1(a)), which can be attributed to recovery during annealing at 573 K. Note that recrystallization is not involved here since aging temperature of 573 K is much lower than the melting temperature of  $\sim\!1890\,\mathrm{K}$  of Ti–12 mass%V alloys.  $^{12}$ 

Figure 2 compares intensity profiles of SAED patterns for the as-rolled alloy and aged alloy after aging at 573 K for 500 h. The intensities were integrated along circumferential direction. <sup>13)</sup> It is noted that all the reflections appeared in the intensity profiles, both as-rolled and aged alloys, can be indexed as those arising from the hexagonal phase, and no reflections of  $\beta$  or  $\omega$  phase are observed. This result indicates that the deformed alloys are still composed of  $\alpha'$  martensite phase including supersaturated V atoms. Reflections become sharp and full width at half maximum (FWHM) is largely reduced after aging, indicating improvement of crystalinity. Actually, FWHM for  $10\bar{1}0$  reflection decreased by half from 0.13 to  $0.065\,\mathrm{nm}^{-1}$ . Thus, the CGR process followed by aging is a novel fabrication method to produce titanium alloys with ultrafine grains.

Figure 3(a) shows an HRTEM image of the as-rolled alloy taken with beam incidence of  $[02\overline{2}1]$ . As seen, there are regions of ~10 nm in size with Moiré fringes at different fringe orientations, indicating distribution of fine grains with slightly different crystallographic orientations. In contrast, local Moiré fringes disappeared after aging at 573 K for 500 h as shown in Fig. 3(b), which was taken at a beam incidence of [5143]. Inset shows a magnified HRTEM image with clear crossed lattice fringes. The disappearance of Moiré fringes is an evidence of atomic diffusion and/or rearrangement of dislocations during annealing at 573 K, which resulted in the improvement of crystalinity as observed in Fig. 2. It is considered that atomic diffusion is limited within a short range since grain sizes are almost the same after aging at 573 K and no reflections of  $\beta$  or  $\omega$  phase have been detected at this stage.

However, in spite of recovery, Vickers hardness increases as aging proceeds. Figure 4 shows changes of Vickers hardness both for STQ and CGR alloys as a function of

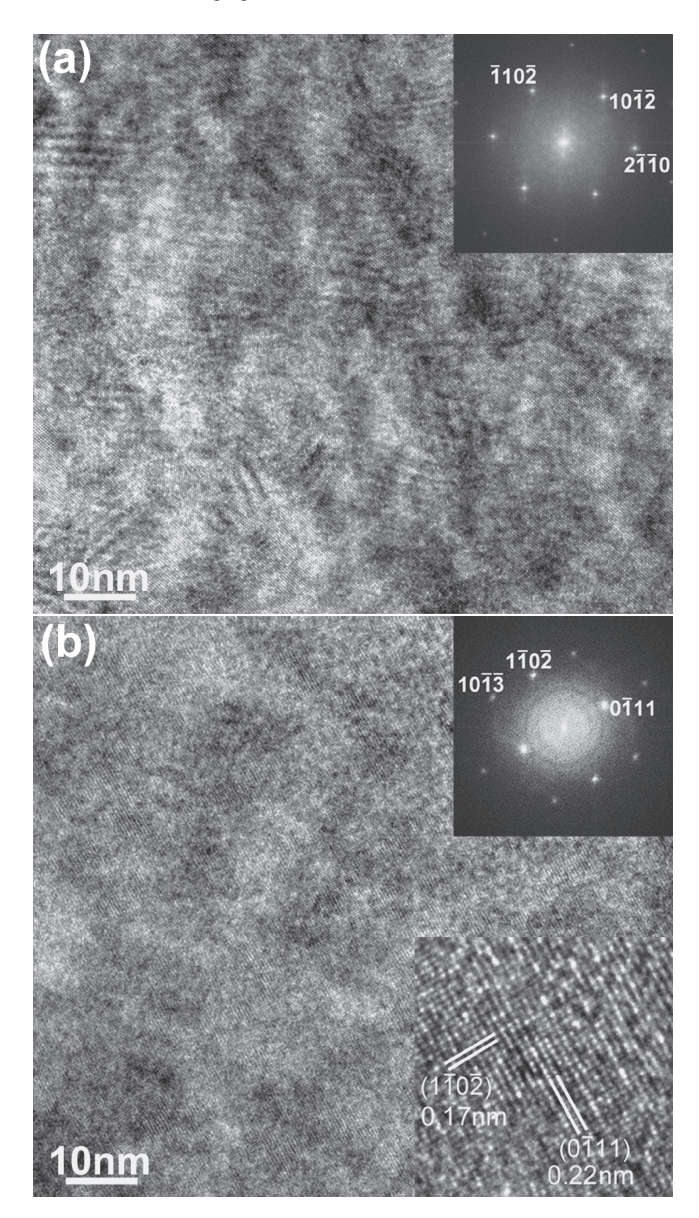


Fig. 3 HRTEM images and the corresponding FFT patterns of CGR alloys; (a) as-rolled, and (b) after aging at 573 K for 500 h. A magnified image is shown in the inset.

holding time at 573 K. The initial hardness of the CGR alloy was 266 H<sub>v</sub>, and it reached 395 H<sub>v</sub> after aging at 573 K for 500 h. Davis et al. reported that the hardness was found to increase markedly with increased interstitial content. 14) The oxygen content of 0.227 mass% for the aged CGR alloy is higher than that for the STQ alloy (0.104 mass%). The initial hardness of 266 H<sub>v</sub> for an as-rolled alloy is higher than that for the aforementioned STQ alloy (205 H<sub>v</sub>) due to work hardening, and comparable to the values (260-280 H<sub>v</sub>) reported for Ti-Mo STQ alloys (2-8 mass%Mo) with similar oxygen content of 2000 ppm (about 0.2 mass%). 14) As the oxygen content largely increased to as high as 2800 ppm, the hardness reached  $\sim$ 330 H<sub>v</sub> (Ti-4%Mo, STQ), which is lower than the value for the aged CGR alloy (395 H<sub>v</sub>) obtained in this study. Thus, the observed age-hardening suggests structural change upon aging rather than interstitial oxygen effect, e.g., phase separation of  $\alpha'$  martensite towards equilibrium  $\alpha$  and  $\beta$  phases. Note that phase decomposition of  $\alpha'$  martensite phase involves partitioning of solute V

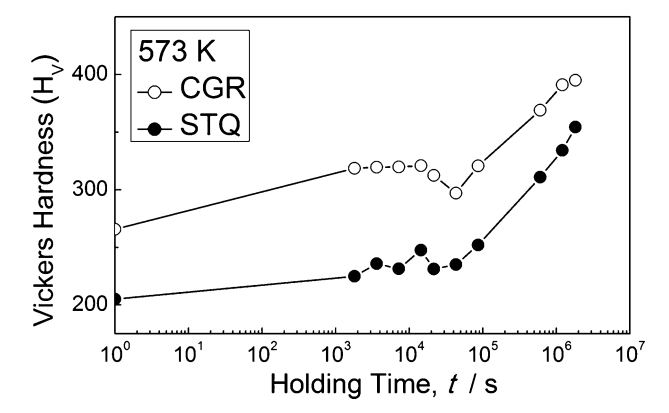


Fig. 4 Change of Vickers hardness at 573 K as a function of holding time both for STQ and CGR alloys.

atoms, while no obvious phase decomposition was detected in the diffraction pattern.

To examine a possible compositional heterogeneity in the aged CGR alloy, we have carried out STEM-EDS elemental analyses as shown in Fig. 5. First, STEM-EDS maps for the as-rolled alloy show homogeneous distribution of Ti, V and Al. In contrast, fine precipitates with V-rich compositions are seen in the alloy after aging at 573 K for 500 h. Size of these precipitates are 10-20 nm and their number density is low at this stage. In the HAADF-STEM image shown in Fig. 5(b), a bright contrast region marked by A contains 61 mass%V (Al content is less than 1%). On the other hand, composition of a dark contrast region marked by B, which is adjacent to the region A, is Ti-1 mass%V-2 mass%A1. Thus, the region B is composed almost of Ti considering a statistical error of EDS measurements. It is worthy to note that partitioning of Ti (Z = 22) and V (Z = 23) atoms upon decomposition of  $\alpha'$ martensite is detected by atomic number (Z) contrast in spite of a quite small atomic number difference. These V-rich and Ti-rich regions are, respectively, equilibrium  $\beta$  and  $\alpha$  phases formed by phase separation of  $\alpha'$  martensite during aging at 573 K. It is plausible that partitioning of solute atoms and formation of fine precipitates can be possible reasons for the age-hardening, however, there are still unsolved questions as follows. First, number density of precipitates detected by the STEM-EDS mapping in Fig. 5(b) is too low as sole origin of the observed hardening. At an early stage of phase separation, precipitates are small and partitioning of solute V atoms is not completed. Therefore, it is considered that only precipitates with a size large enough containing a certain amount of V can be detected by STEM-EDS analyses. On the other hand, most of the smaller precipitates with less V contents will be difficult to precisely detect by using EDS. Secondly, it is also difficult to distinguish  $\alpha'$  martensite and precipitated  $\alpha$  phase in the aged CGR alloys since these two phases are quite similar in structure (hcp) with only slightly different solute concentrations.

To further clarify the evolution of phase separation process, we have observed microstructures of the CGR alloy aged at higher temperatures. Figure 6(a) shows an SAED pattern of the alloy aged at 673 K for 24 h taken from an area of  $\sim$ 800 nm in diameter. The pattern shows discontinuous rings and all reflections can be indexed as those of the hcp structure. On the other hand, the  $\beta$  phase was detected from a local area

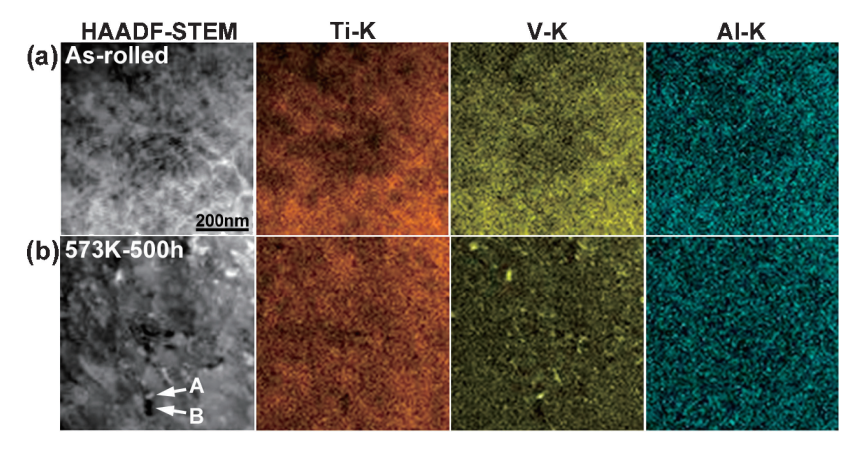


Fig. 5 STEM-EDS elemental maps of a CGR alloy; (a) as-rolled, and (b) after aging at 573 K for 500 h.

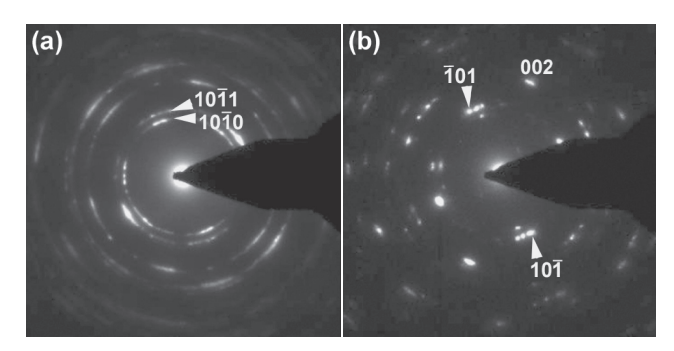


Fig. 6 (a) An SAED pattern of a CGR alloy after aging at 673 K for 24 h. (b) A diffraction pattern taken from a local area with the beam incidence of [010]<sub>β</sub>.

(about 200 nm in diameter) as shown in Fig. 6(b). Formation of the  $\beta$  phase indicates partitioning of solute atoms towards equilibrium V-deficient  $\alpha$  (hcp) and V-rich  $\beta$  (bcc) phases.

Figure 7 shows an HRTEM image at  $\alpha/\beta$  grain boundary of a specimen after aging at 673 K for 24 h. The upper left corner of the image corresponds to an area of the  $\beta$  phase characterized by crossed {101} lattice fringes (zone axis: [010]), while the lower right corner corresponds to the area of the  $\alpha$  phase with (1101) fringes (zone axis: [1011]). As seen, Moiré fringes exist at  $\alpha/\beta$  grain boundary. This HRTEM image and the corresponding Fast Fourier Transform (FFT) pattern indicate the following orientation relationship (OR) between precipitated  $\beta$  and  $\alpha$  phases:  $(101)_{\beta}$  //  $(01\bar{1}\bar{1})_{\alpha}$ ,  $[010]_{\beta}$  //  $[10\bar{1}1]_{\alpha}$ . This OR has been observed in an STQ alloy followed by aging at 673 K for 24 h. 11) After aging at 773 K for 24 h, in addition to the above OR, the Burgers' OR,  $(0001)_{\alpha}$  //  $(1\bar{1}0)_{\beta}$ ,  $[\bar{1}2\bar{1}0]_{\alpha}$  //  $[111]_{\beta}$ , was also observed. 15) It should be noted that the Burgers' OR has been reported for  $\alpha$  precipitates in the  $\beta$  matrix of Ti–Mo alloys, 9) suggesting similarity between  $\beta$  precipitates in the  $\alpha'$ matrix and  $\alpha$  precipitates in the  $\beta$  matrix.

Figure 8 shows results of STEM-EDS elemental mapping for the alloy after aging at 673 K for 24 h. Distribution of the  $\beta$  precipitates,  $\sim$ 50 nm in sizes, are seen in the HAADF-STEM image as well as in the V-K map. Note that Z-contrast imaging of HAADF-STEM is quite useful to detect V-rich  $\beta$  precipitates, which can be identified by bright contrasts. The EDS mapping thus clearly shows that phase decomposition of  $\alpha'$  martensites proceeded towards the equilibrium  $\alpha$  and  $\beta$  phases during the aging at 673 K.

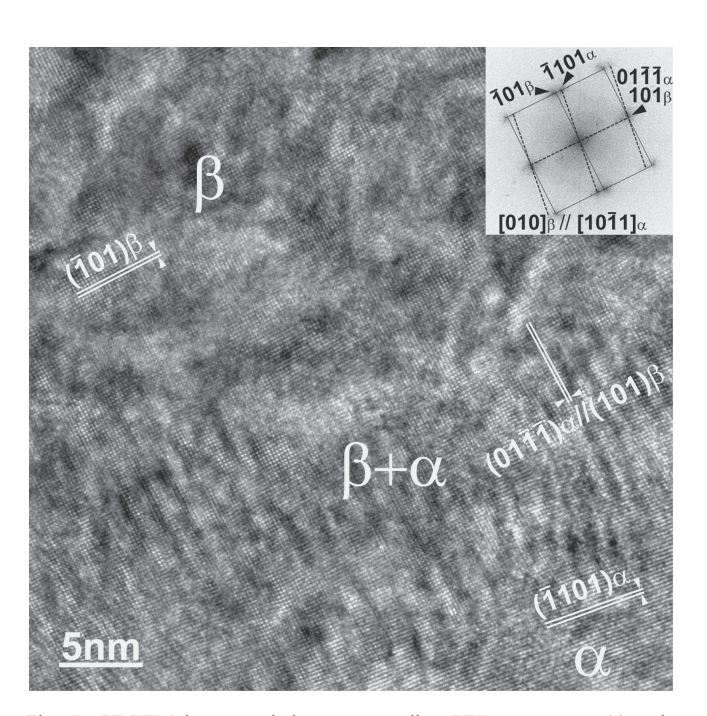


Fig. 7 HRTEM image and the corresponding FFT pattern at  $\alpha/\beta$  grain boundary of a CGR alloy after aging at 673 K for 24 h. The beam incidence is  $[010]_{\beta}$  and  $[10\bar{1}1]_{\alpha}$ .

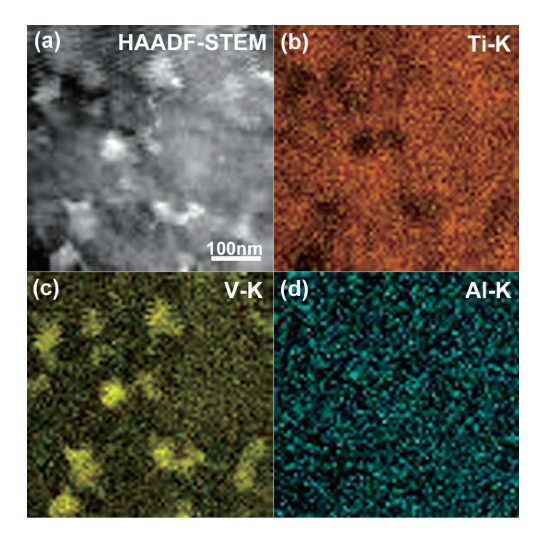


Fig. 8 STEM-EDS elemental mapping for a CGR alloy after aging at 673 K for 24h. (a) HAADF-STEM image, (b) Ti-K map, (c) V-K map, and (d) Al-K map.

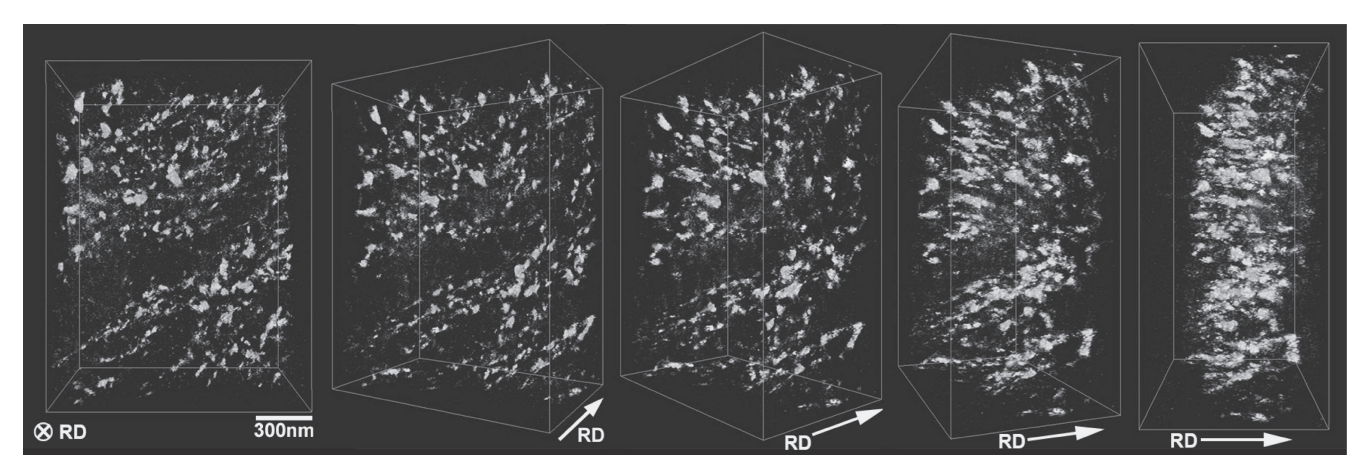


Fig. 9 Three-dimensional views of the β precipitates in a CGR alloy after aging at 673 K for 24 h reconstructed from a HAADF-STEM tilt-series dataset using a WBP technique.

To elucidate three-dimensional (3D) distribution of the  $\beta$ precipitates, we have carried out electron tomography. The 3D structures were reconstructed using a tilt-series data set of 2D HAADF-STEM images taken at tilt angles between -60 and  $+60^{\circ}$ . It is noted that SAED patterns showed discontinuous Debye-Scherrer rings during the tilting, which is a proof of overall polycrystalline nature of the aged CGR alloy. The tilt angle increments were set 2° for angle range of 0 to  $|50|^{\circ}$ , and 1° for  $|50|^{\circ}$  to  $|60|^{\circ}$ . The reconstructed volume is  $1420 \,\mathrm{nm} \times 1876 \,\mathrm{nm} \times 926 \,\mathrm{nm}$  (368 pixels  $\times$  486 pixels  $\times$ 240 pixels) with the pixel size of 3.86 nm/pixel. Figure 9 shows reconstructed 3D images of the alloy after aging at 673 K for 24 h. Precipitates, 30–70 nm in size, correspond to the V-rich  $\beta$  phase, since the original images are essentially the Z contrast, as shown by the precipitated  $\beta$  phase imaged as bright contrasts in Fig. 8(a). As seen, spatial distribution of fine  $\beta$  precipitates is not random but rather aligned, indicating a heterogeneous nucleation and growth of  $\beta$  precipitates in the deformed  $\alpha'$  matrix.

#### 4. Conclusion

We have characterized microstructures of  $\alpha'$  martensite in Ti–12 mass%V–2 mass%Al alloys deformed by CGR and their structural evolution on aging by using TEM, STEM and electron tomography. The results can be summarized as follows.

- (1) Acicular structure of hexagonal  $\alpha'$  martensite changes into fine equiaxed  $\alpha'$  grains by CGR with a cold reduction of 75%. After aging at 573 K for 500 h, local Moiré fringes disappear and diffraction rings become sharp due to recovery.
- (2) Vickers hardness increases, reaching 395 H<sub>v</sub>, by aging at 573 K in spite of the recovery. It is suggested that partitioning of solute atoms and the formation of fine precipitates are among the possible reasons for the agehardening.
- (3) Following OR is observed locally between precipitated  $\beta$  and  $\alpha$  phases after aging at 673 K:  $(101)_{\beta}$  //  $(01\bar{1}\bar{1})_{\alpha}$ ,  $[010]_{\beta}$  //  $[10\bar{1}1]_{\alpha}$ .
- (4) Distribution of  $\beta$  precipitates in the CGR alloys aged at 673 K for 24 h was observed by STEM-EDS elemental mapping and electron tomography. Reconstructed 3D

images revealed a heterogeneous nucleation and growth of  $\beta$  precipitates in the deformed  $\alpha'$  matrix.

#### Acknowledgments

The authors wish to thank Mr. K. Kodaira for his contribution in this study, Mr. E. Aoyagi and Mr. Y. Hayasaka of Tohoku University for their help using TEM. This study was partly supported by the Grant-in-Aid for Scientific Research on Innovative Area, "Bulk Nanostructured Metals" (No. 25102703) from the Ministry of Education, Culture, Sports, Science and Technology, and Japan Science Technology Agency "Development of systems and technology for advanced measurement and analysis" program. KS appreciate financial supports from the General Sekiyu R & D Encouragement Assistance Foundation and the Kazato Research Foundation.

#### REFERENCES

- E. W. Collings: The Physical Metallurgy of Titanium Alloys, (ASM, Metals Park, Ohio, 1984).
- 2) G. Lutjering and J. C. Williams: Titanium, (Springer, Berlin, 2003).
- 3) M. Niinomi: Metall. Mater. Trans. A 33 (2002) 477-486.
- H. Matsumoto, S. Watanabe, N. Masahashi and S. Hanada: Metall. Mater. Trans. A 37 (2006) 3239–3249.
- H. Matsumoto, S. Watanabe and S. Hanada: Mater. Sci. Eng. A 448 (2007) 39–48.
- H. Matsumoto, K. Kodaira and A. Chiba: J. Japan. Inst. Metals 72 (2008) 989–996.
- H. Matsumoto, K. Kodaira, K. Sato, T. J. Konno and A. Chiba: Mater. Trans. 50 (2009) 2744–2750.
- H. Matsumoto, H. Yoneda, D. Fabregue, E. Maire, A. Chiba and F. Gejima: J. Alloy. Compd. 509 (2011) 2684–2692.
- T. Furuhara, T. Makino, Y. Idei, H. Ishigaki, A. Takada and T. Maki: Mater. Trans. JIM 39 (1998) 31–39.
- M. J. Donachie, Jr.: Titanium A Technical Guide 2nd ed., (ASM International, Materials Park, Ohio, 2000) pp. 13–24.
- K. Sato, H. Matsumoto, K. Kodaira, A. Chiba and T. J. Konno: J. Alloy. Compd. 506 (2010) 607–614.
- 12) J. Labár: Microsc. Microanal. 14 (2008) 287–295.
- 13) H. Okamoto: J. Phase Equilibria. 14 (1993) 266-267.
- R. Davis, H. M. Flower and D. R. F. West: J. Mater. Sci. 14 (1979) 712–722.
- K. Sato, H. Matsumoto, A. Chiba and T. J. Konno: Proc. 15th European Microscopy Congress, 1 (2012) pp. 409–410.